The 9th European Congress on Computational Methods in Applied Sciences and Engineering
ECCOMAS Congress 2024
3–7 June 2024, Lisboa, Portugal

TIME-DEPENDENT FLOW SIMULATION OF THIXOTROPIC CEMENTITIOUS PASTES

MAREIKE THIEDEITZ[1] AND JITHENDER J. THIMOTHY[1]

[1] Technical University of Munich;
TUM School of Engineering and Design,
Department of Materials Engineering,
Center for Building Materials,
e-mail: jithender.timothy@tum.de

Key words: Thixotropy, Cement paste, Time-dependent flow, Computational Fluid Dynamics

Summary. Understanding the flow of cementitious pastes is essential for optimizing their processing and application in construction, ensuring material performance and structural integrity. Computational Fluid Dynamics (CFD) provides deeper insights by enabling the detailed simulation and analysis of the complex, time-dependent flow behaviors of cementitious pastes, which are difficult to capture through experimental methods alone. However, the computational investigation of time- and shear rate-dependent transient properties in increasingly non-Newtonian and thixotropic cementitious pastes remains unexplored due to its significant challenges. This research investigates the transient properties of a thixotropic cementitious paste rheologically, in experimental flow tests and computationally using CFD. The slump flow test and the L-Box test were performed to analyze the cement paste flowability, and subsequently replicated in a CFD simulation using OpenFOAM. The paste thixotropy, characterized by structural buildup and breakdown, was analyzed with rheometry. A regularized thixotropy model with viscoplastic Herschel-Bulkley flow and a structural parameter λ was implemented into OpenFOAM to model the time- and shear rate- dependent paste flow. The numerical simulation of the flow tests was analyzed with special regards to transient processes and the evolution of the structural parameter. The thixotropy parameters flocculation time and structural breakdown value were found to affect the flow progress independent of time during slow flow. Thixotropy parameters investigated in the lab could approximate the simulated flow in comparison to the real flow. The time-dependent L-Box flow was affected by thixotropy rather than the fast-stopping slump flow test. Prospectively, an explicit thixotropy modeling can considerably improve the accuracy of the simulation of time-dependent flow phenomena of cementitious building materials.

1 INTRODUCTION

The numerical simulation of concrete flow enables the prediction, adjustment, and optimization of concrete processing by applying transport equations from fluid dynamics, typically through Computational Fluid Dynamics (CFD), or by utilizing the fundamental principles of solid mechanics, particularly through Discrete Particle Modeling (DPM). Numerical calculations have enabled researchers to estimate the final flow result of poured concrete, especially Self-Compacting Concrete (SCC) [26], material properties during pumping [11], or the buildability of layered concrete in Additive Manufacturing processes. Furthermore, numerical methods

facilitate the investigation of the shear rate distributions during mixing [27]. Frequently, the standardized workability tests slump flow test according to DIN EN 1015-3 [8] and DIN EN 12350-8 [10] or the L-Box test according to DIN EN 12350-10 [9] are replicated in numerical simulations to validate rheological models or the numerical framework.

However, while the numerical simulation of concrete flow has become popular, the implementation of rheological properties into numerical models is still a field of ongoing research [18, 13]. Many state-of-the-art numerical simulations do not account for the flow properties of modern concrete mixtures such as SCC, Ultra-High-Performance Concrete (UHPC) and ecological concretes with reduced clinker amounts. Due to a higher fraction of fine and reactive particles in the cementitious paste matrix, a higher amount of chemical admixtures and lower water-to-cement (w(c) [15], these concretes increasingly incorporate non-linear viscosities, viscoelastic contributions and time- and shear rate- dependent thixotropic structural buildup [12, 2, 1]. First thixotropy-implemented rheological models have been tested in simulation setups of concrete flow, such as [6, 7]. However, the effect of thixotropy on time-dependent flow is yet to be investigated. Therefore, this research analyses thixotropic properties of cementitious pastes on their effect on the slump flow test and the L-Box test. It combines the rheometric analysis and rheological modeling of transient thixotropy of a densely packed cementitious suspension with the CFD analysis of free-surface cementitious paste flow, and compares the results with experimental flow tests.

2 MATHEMATICAL FUNDAMENTALS

2.1 Thixotropy of cementitious pastes

Cementitious pastes are colloidal, multi-phase suspensions. Once the particle solid volume fraction Φ_s surpasses the percolation threshold, particle interactions occur and the cementitious paste exhibits a yield stress τ, a structural viscosity η and, depending on the particle network strength and particle interactions, thixotropic structural buildup or breakdown, which is the time-dependent change of viscosity [5, 19]. As the cementitious paste undergoes constant microstructural alterations due to the hydration reaction, it incorporates both reversible thixotropy and irreversible structural buildup [20]. The constitutive equation for shear stress τ that depends on both the shear rate and thixotropy was proposed by [4]:

$$\tau \quad = \quad \tau(\dot{\gamma}, \lambda); \frac{d\lambda}{dt} = -k_1\dot{\gamma}\lambda + k_2(1-\lambda) \tag{1}$$

In Eq. 1, λ is the structural parameter which can be calculated as a temporal derivative depending on the shear rate $\dot{\gamma}$, a structural breakdown parameter k_1, and the structural buildup parameter k_2. For the modeling of cement and concrete thixotropy, [5] formulated a similar calculation of λ:

$$\frac{d\lambda}{dt} = \frac{1}{T\lambda^m} - \alpha\lambda\dot{\gamma} \tag{2}$$

With T as characteristic flocculation time in seconds, α as structural breakdown parameter and m as scaling factor. Based on Eq. 2, [17] formulated a simplified rheological equation implementing the structural parameter λ into the Herschel-Bulkley model for viscoplastic flow:

$$\tau(\dot{\gamma}) = (1+\lambda)\tau_{0,H.-B.} + k\dot{\gamma}^n \tag{3}$$

In Eq. 3, $\tau_{0,H.-B.}$ is the dynamic Herschel-Bulkley yield stress in Pa, k is a consistency index in Pas^n and n is the dimensionless non-Newtonian index indicating shear-thinning flow when $n < 1$, Bingham flow when $n = 1$ and shear-thickening flow when $n > 1$.

2.2 Numerical modeling of free-surface paste flow

CFD uses numerical algorithms to solve the Navier-Stokes transport equations of viscous fluid flow. Most available CFD software discretize the Navier-Stokes equations for a two- or three-dimensional mesh using the Finite-Volume-Method (FVM). To simulate free-surface flow, the Volume-of-Fluid method (VOF) is used. In VOF, the Navier-Stokes equations are extended by the quantity α that weights the phases in dependence on their fluid density:

$$\rho = \alpha\rho_1 + (1 - \alpha)\rho_2 \tag{4}$$

The continuity equation yields:

$$\frac{\partial\alpha}{\partial t} + \nabla \cdot (\alpha\mathbf{u}) = 0 \tag{5}$$

The momentum equation yields Eq. 6:

$$\frac{\partial\rho\mathbf{u}}{\partial t} + \nabla \cdot (\rho\mathbf{u}\mathbf{u}) = -\nabla p + \nabla \cdot \tau + \rho g + f_\sigma \tag{6}$$

In Eq. 6, ρ is the fluid density in kg/m^3, $\mathbf{u}$ is the velocity vector in m/s, p is the scalar pressure in Pa, τ is the deviatoric stress tensor in Pa, g is the gravitational acceleration in m/s^2, and f_σ is the contribution from surface tension effects between the two phases [3]. When implementing yield stress models for $\nabla \cdot \tau$ to solve material-dependent flow, the numerical solution becomes unstable, because no solution for $\dot{\gamma} = 0$ exists. Therefore, rheological models must be regularized for a continuous solution towards $\dot{\gamma} \to 0$. Comprehensive reviews on regularization methods are found in [21].

3 EXPERIMENTAL AND NUMERICAL FRAMEWORK

This study combines the rheological investigation of cementitious paste thixotropy using rheometry and experimental flow tests with a numerical simulation approach. While the aim is to implement experimental rheological parameters into the numerical framework, arbitrary thixotropy parameters as variation to the experimentally measured and calculated rheological values are tested as well.

Cementitious paste with a solid volume fraction $\Phi_s = 0.55$, which equals a w/c ratio of 0.26, was prepared with an Ordinary Portland Cement (OPC) CEM I 0.42 R, Heidelberg Materials, Germany, and deionized water. The paste composition is shown in Table 1. The paste temperature was 20°C. The flowability was adjusted by the addition of polycarboxylather as superplasticizer (PCE) with 1.40 % by weight of cement (bwoc).

The cementitious paste was mixed for 90 seconds with a hand-drilling machine at 1700 rpm. The paste was left at rest for 11 min and sheared again for 30 seconds. Experimental flow tests and the rheological characterization through rheometry were conducted 15 minutes after water addition.

Table 1: Cement paste composition

Mixture	Φ_s	w/c ratio	CEM I	Water	PCE	ρ_p
	[-]	[-]	[kg/m^3]	[kg/m^3]	[%] bwoc	[kg/m^3]
OPC−0.55	0.55	0.26	1710.5	450	1.40	2160

3.1 Experimental flow tests

In a mini slump flow test using the Hägermann cone according to DIN EN 1015-3 [8], the paste exhibited a slump flow value of 250 mm after less than two seconds of flow time, see Figure 1 (a). In a mini L-Box test according to DIN EN 12350-10 [9] but with modified L-Box dimensions, see [23], the paste showed a final flow length of 435 mm after 20 seconds of flow, see Figure 1 (b). Slow creeping continued after the measurement time. The L-Box flow was recorded.

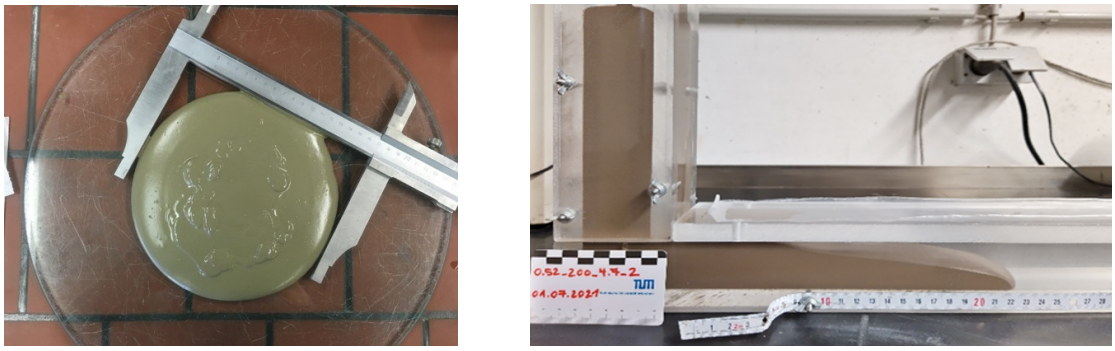

(a) Slump flow (b) L-Box flow

Figure 1: Flow tests: (a) Measurement of the slump flow diameter, (b) Flow body in the L-Box

3.2 Rheometric analysis

Rheometric tests were conducted in the rheometer MCR 502 by Anton Paar, Germany. Parallel plates with a diameter of 50 mm, serrated surfaces and a gap height of 1 mm were used. The rheometric tests comprised of a full rheological characterization to describe a material's stress response $\tau(t)$ as function of $\dot{\gamma}$ and λ, depicted by Eq. 2. The rheological characterization is introduced shortly. Detailed information on the measurement method, raw data treatment and viscoplastic modeling are available in the author's publication [24]. The structural buildup model for λ and its experimental validation are elaborated in the author's publication [22].

The measurement profile and material response of the rotational dynamic shear rate test are illustrated in Figure 2. The shear rate profile comprised of a pre-shear at $\dot{\gamma} = 40$ s^{-1} for 30 seconds, followed by a stepwise decreasing rate profile from $\dot{\gamma} = 80$ s^{-1} to 0.02 s^{-1}. The shear stress per rate step was calculated as the equilibrium of each step. Subsequently, the $\dot{\gamma} - \tau$ flow curve was plotted, see Figure 2 (b). The critical shear rate $\dot{\gamma}_{crit}$ was defined as the shear rate where τ exhibited a minimum. The Herschel-Bulkley regression was applied to the flow curve

in the range of $\dot{\gamma} > \dot{\gamma}_{crit}$:

$$\tau = \tau_{0,d} + k\dot{\gamma}^n \tag{7}$$

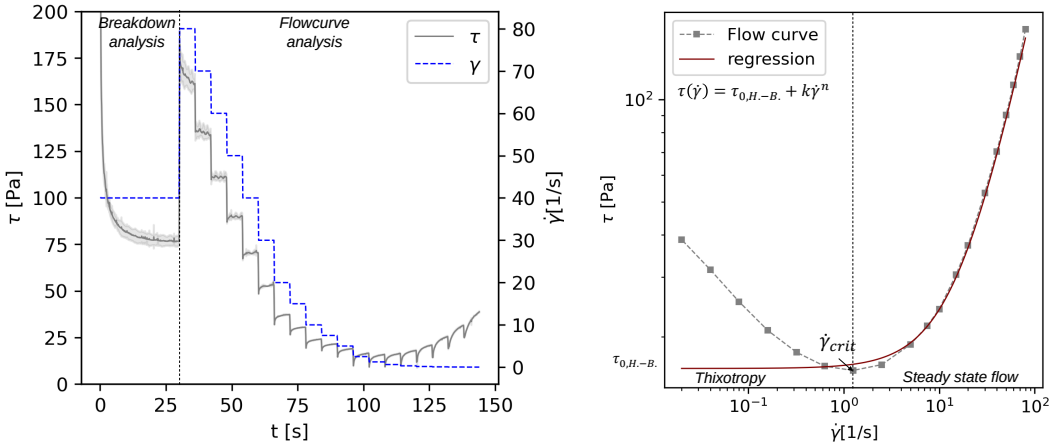

(a) Stress response to shear rate profile

(b) Calculated $\dot{\gamma} - \tau$ flowcruve with regression

Figure 2: Dynamic rotational shear test to investigate rheological flow parameters yield stress τ_0, the viscosity and the structural breakdown parameter

A structural breakdown parameter α was calculated by applying Eq. 8 as the first part of Eq. 2 on the stress evolution $\tau(t)$ at $\dot{\gamma} = 40$ s^{-1}:

$$\tau(t) \quad = \quad \tau \frac{d\lambda}{dt}; \frac{d\lambda}{dt} = -\alpha\dot{\gamma}\lambda \tag{8}$$

Structural buildup was investigated by applying a small amplitude oscillatory shear protocol as illustrated in Figure 3. A low strain of $\gamma = 5{\cdot}10^{-3}\%$ was applied to the paste as non-destructive strain amplitude. Consequently, the increasing storage modulus G' and loss modulus G'' were measured over a period of 20 minutes. Figure 3 (a) illustrates the measured raw data and the evolution of the phase shift angle δ, which is calculated as $\delta = \tan \frac{G''}{G'}$.

Different theories exist on the assessment of buildup parameters and the flocculation time. In this framework, the buildup curve of the storage modulus $G'(t)$ was fitted to Eq. 9, which was adopted from Ma [14] and elaborated by the author in [22]:

$$G'(t) = \begin{cases} G'_0 + c\lambda(t) & \text{for } t \in [0;\Theta] \\ G'_{0,rig} + G_{rig}t & \text{for } t \in [0;t_{max}] \end{cases} \tag{9}$$

In Eq. 9, the evolution of G' is divided into a structural buildup part driven by flocculation for $t \in [0;\Theta]$ with c as flocculation parameter and λ as structural parameter, and a second buildup part driven by rigidification with G_{rig} as rigidification rate in Pa/s. As no structural breakdown occurs during the non-destructive measurement technique, the explicit solution for the structural buildup-dependent evolution of the storage modulus yields:

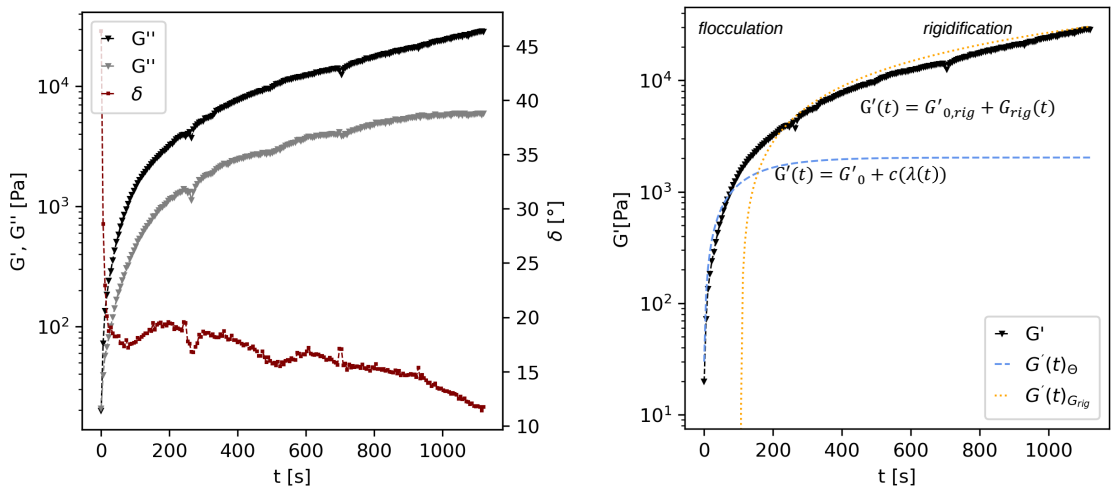

(a) Measured data of G', G'' and δ

(b) Structural buildup analysis

Figure 3: Oscillatory protocol in the non-destructive strain amplitude regime

$$G'(t) = G'_0 + c(\lambda_0 - 1)e^{-\frac{t}{\Theta}} \tag{10}$$

Where λ_0 is the start condition and Θ is the flocculation time in s. The regression fits for Eq. 9 are exemplified in Figure 3 (b).

The Herschel-Bulkley parameters $\tau_{0,H.-B.}$, k and n, structural breakdown α and the flocculation time Θ were subsequently implemented into Eq. 3.

3.3 Numerical framework

The numerical simulations were carried out with the software OpenFOAM (Open-source Field Operation And Manipulation, `https://openfoam.org`), version 7 (dated July 8, 2019), to solve the Navier-Stokes equations with the Volume-of-Fluid (VoF) method. For simulating free-surface flow, OpenFOAM employs the PIMPLE algorithm to couple pressure and velocity. Geometries for the slump test and the L-Box flow test were created using the meshing software GMESH and BLENDER. Since the cone geometry in the slump test is axi-symmetric, it was implemented as a two-dimensional slice with a rotational angle of 3 degrees. Convergence analysis was conducted beforehand and is documented in [25]. The L-Box was designed to closely resemble reality as a three-dimensional body, as shown in Figure 4. Mesh information are summarized in Table 2.

The boundary velocity $\mathbf{u}$ at fixed walls was set as a Dirichlet condition, with a value of 0, while no additional pressure p was defined apart from gravity. All other boundary conditions were specified as Neumann conditions, with a value of zero. User-dependent artifacts resulting from both test procedures (lifting the gate in an L-Box test and lifting the cone for slump flow measurements) were not considered. The Papanastasiou regularization method, proposed by [16], was chosen as a mathematical blending function. Previous studies by the authors investigated the optimization of regularization methods and parameters [25]. The final implementation of the regularized transport model for non-Newtonian thixotropic paste flow is described by Eq. 11:

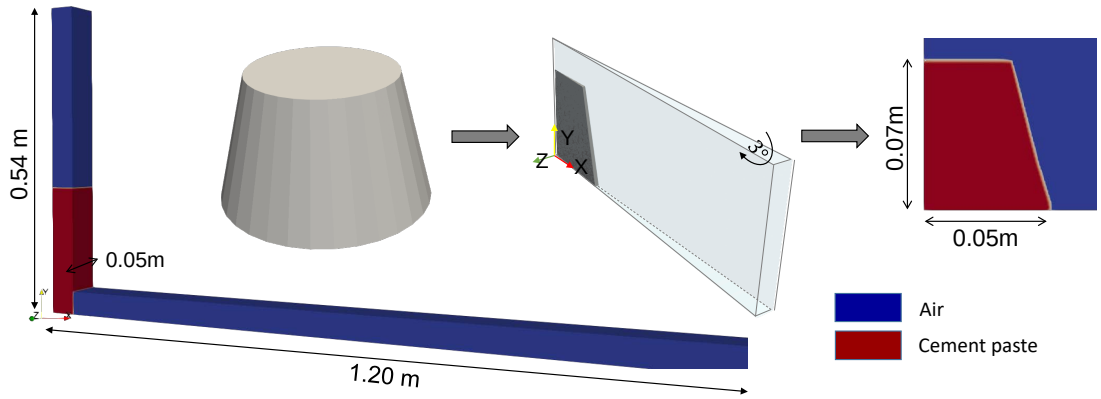

Figure 4: OpenFoam geometries of flow tests: Three-dimensional L-Box and slice geometry of the slump cone with cement paste at t = 0 s

Table 2: Geometrical mesh parameters

Geometry	Δ x	Δ y	Δ z	Angle	Aspect ratio	Σ Cells
	[m]	[m]	[m]	[°]	[-]	[-]
Slice	0.0005	0.0005	x	3	1	63,441
L-Box	0.001	0.001	0.001	x	1	312,500

$$\eta(\dot{\gamma}) = \frac{(1+\lambda)\tau_0(1-e^{-m\frac{\dot{\gamma}}{\dot{\gamma}_{crit}}})}{\dot{\gamma}} + k\dot{\gamma}^{n-1} \tag{11}$$

In Eq. 11, the shear-rate dependent viscosity $\eta(\dot{\gamma})$ is calculated by the thixotropy-implemented Herschel-Bulkley model, which is blended by the Papanastasiou regularization with m as dimensionless blending parameter. $\dot{\gamma}_{crit}$ is the critical shear rate. λ is the structural parameter, which is calculated as shear rate and time - dependent derivative. In OpenFOAM, the variable S was employed as structural derivative according to Eq. 2, developed in the OpenFOAM framework by de Schryver, see [7].

The experimentally investigated parameters for the numerical simulation are collected in Table 3. To investigate the effect of thixotropy parameters on the numerical flow simulation, the structural buildup and breakdown parameters, implemented as flocculation time T and breakdown value α, were varied.

4 RESULTS

4.1 Simulation results for the flow evolution

The results for all flow simulations with varying thixotropy parameters are illustrated in Figure 5 as the evolution of the slump radius over time (see Figure 5 (a)) and the evolution of the flow length in the L-Box simulation (see Figure 5 (b)), with the deflocculation parameter α labeled as "-a0.x". Figure 5 (a) illustrates that variations in thixotropy parameters do not

Table 3: Rheological parameters from regression analysis

Test series	$\tau_{0,H.-B.}$	k	n	$\dot{\gamma}_{crit}$	T	α	m
	[Pa]	[Pa∗s^n]	[-]	[s^{-1}]	[s]	[-]	[-]
OPC−0.55$_{exp}$	16.4	0.29	1.41	1.25	120	0.14	1000
OPC−0.55-T-α	16.4	0.29	1.41	1.25	50 100 200 500	0.1 0.15 0.2	1000

significantly affect the final flow radius in a slump flow test. The experimental result closely matches the simulated flow after 1 second of simulation time, with negligible variations observed over time. On the other hand, Figure 5 (b) demonstrates the influence of thixotropy parameters on flow evolution in a simulated L-Box test.

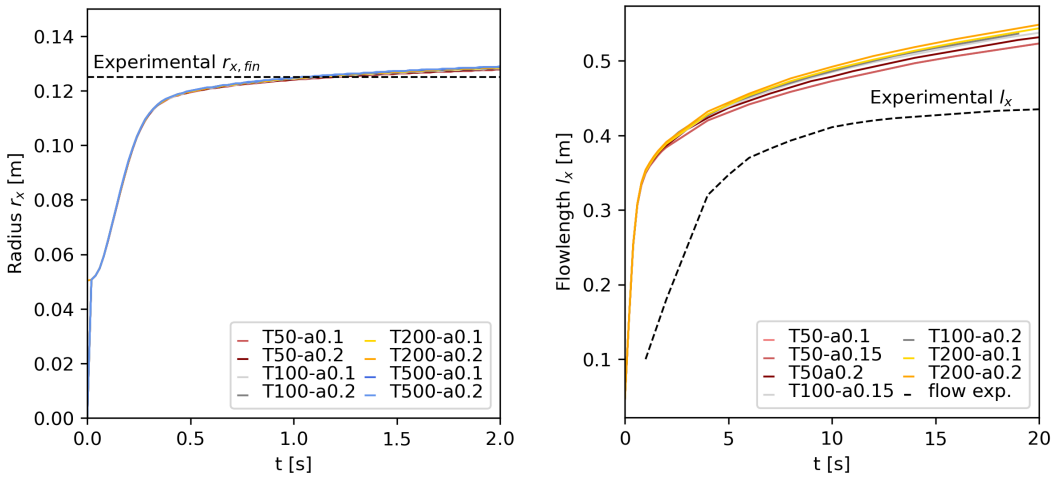

(a) Numerical slump flow results

(b) Numerical L-Box flow results

Figure 5: Flow over time results for different thixotropy parameters for both geometries

All L-Box simulation results surpass the experimental flow test, possibly due to secondary effects like wall interactions in the experimental test. Further analysis of this discrepancy is beyond the scope of this publication. After several seconds of flow, the flow behavior depends on the model parameters T and α. Longer flocculation times and higher values of α, indicating stronger deflocculation, lead to faster flow evolution. Conversely, increased thixotropy reduces flow velocity.

For a more detailed analysis of transient flow properties, refer to Figure 6 and Figure 7. The shear rate distribution $\dot{\gamma}$ and the structural parameter, denoted in the numerical simulation as S, are visualized for the simulation cases T50-a0.1 over the two-dimensional shapes, the maximum values are plotted in the diagrams. Histograms with a bin value of 100 in the figures illustrate the

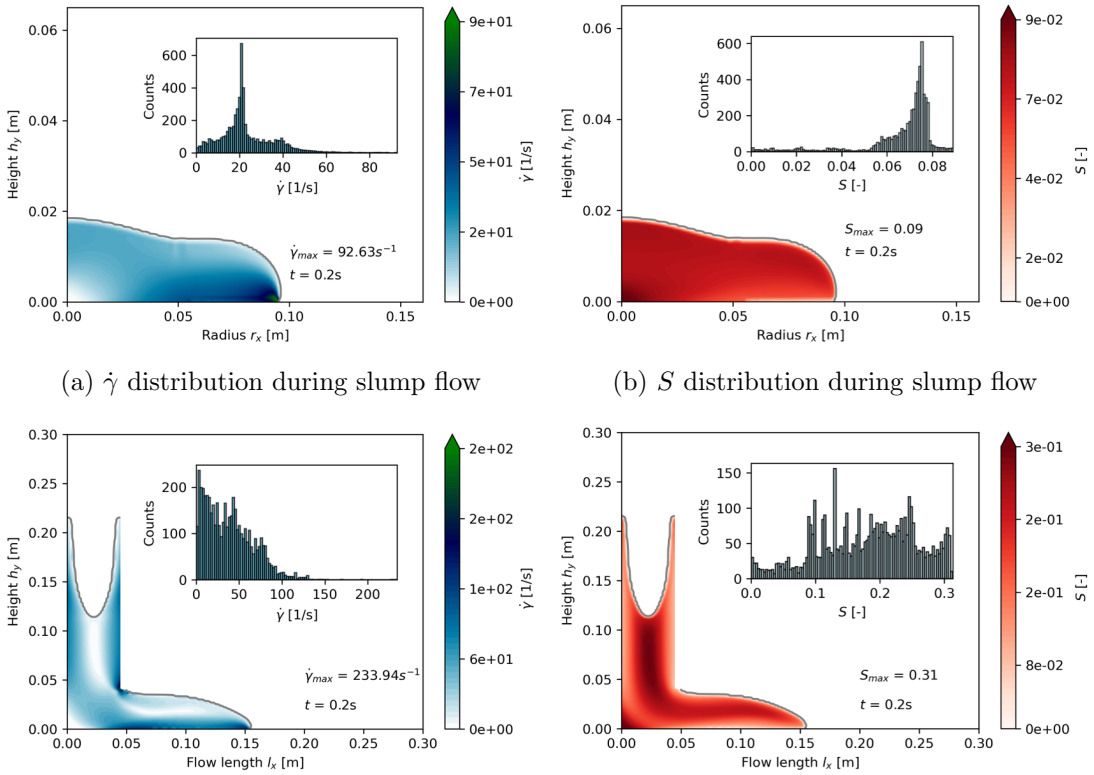

(a) $\dot{\gamma}$ distribution during slump flow

(b) S distribution during slump flow

(c) $\dot{\gamma}$ distribution during L-Box flow

(d) S distribution during L-Box flow

Figure 6: Two-dimensional shear rate and structural buildup distribution after 0.2 seconds of flow

density distribution of $\dot{\gamma}$ and S over the cells of the two-dimensional slice. Figure 6 illustrates the initial flow properties at 0.2 seconds of flow. Figure 7 visualizes late flow properties at 1 second of the slump flow and 10 seconds of L-Box flow, respectively. Figure 6 demonstrates that in both tests, the paste does not flow at r_x and $l_x = 0$. Shear rates increase towards the flow direction. Higher shear rates are apparent in the L-Box, possibly due to a higher pressure field originating from higher gravitational forces and increased acceleration onto the paste. Still, already after 0.2 seconds of flow, higher structural values S exist in the L-Box, with $S_{max} = 0.31$ compared to a maximum value of $S_{max} = 0.09$ in the slump test. Furthermore, the density distribution illustrates the broad variation of S values over the two-dimensional shape of the L-Box compared to the S distribution in the slump shape.

Late flow properties are visualized in Figure 7. As the slump test approaches its final value fast, time-dependent structural buildup has little chance to affect the flow properties. The structural parameter has only increased towards a maximum value of $S_{max} = 0.2$. In the L-Box test, the structural parameter has increased to $S_{max} = 0.7$, with a high density of S between 0.4 and 0.6, as illustrated in the density histogram. The flow proceeds slow and at low shear rates. However, as illustrated in Figure 5 (b), does the flow in the L-Box proceed longer. Rheological parameters, thus, are increasingly affected by the evolution of S.

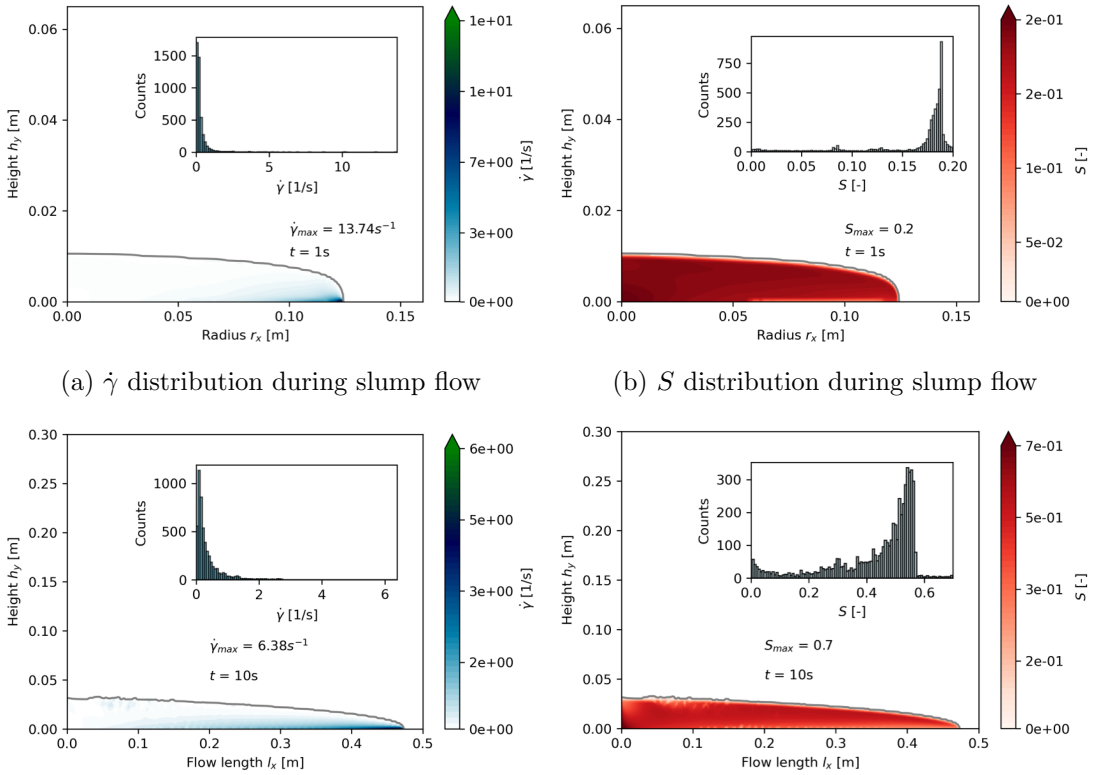

(a) $\dot{\gamma}$ distribution during slump flow

(b) S distribution during slump flow

(c) $\dot{\gamma}$ distribution during L-Box flow

(d) S distribution during L-Box flow

Figure 7: Two-dimensional shear rate and structural buildup distribution after 0.2 seconds of flow

4.2 The effect of thixotropy parameters on transient flow properties

Figure 8 shows the evolution of the structural parameter. Two values for all simulation cases were calculated: Once, only the maximum structural value S_{max} for each calculated time step is illustrated. The virtual value S_{cum} demonstrates the calculated area under the density distribution previously illustrated in the histograms of Figure 6 and Figure 7.

The flocculation time T affects the structural parameter significantly: With decreasing flocculation time, structural buildup proceeds stronger. The deflocculation parameter α shows little influence on both the maximum structural value S_{max} and on S_{cum}. However, deflocculation also affects local flow properties significantly, which becomes visible in Figure 9. The local distribution of S is visualized for the L-Box flow cases T200-a0.1 and T200-a0.2. The histograms show that while S_{max} is similar, the distribution of S varies. The test series T200-a0.1 with a weaker deflocculation parameter possesses higher structural buildup values towards $S = 0.2$, while T200-a0.2 has its highest value frequency around $S = 0.1$.

5 SUMMARY AND CONCLUSIONS

The research introduces an experimental approach to measure thixotropy based on a time- and shear rate- dependent model for the structural parameter λ. This model was then incorporated

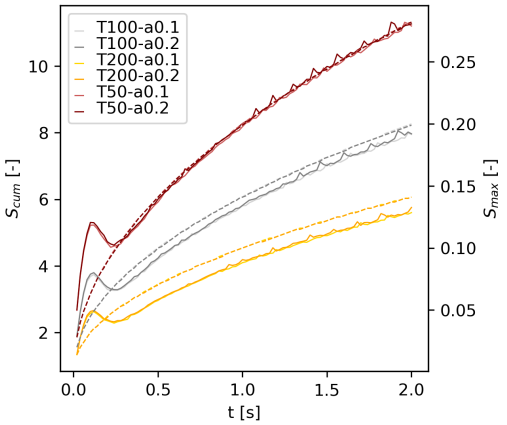

(a) Numerical slump flow results

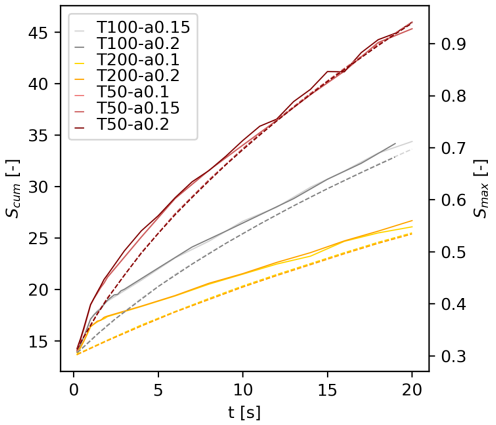

(b) Numerical L-Box flow results

Figure 8: Evolution of structural parameter over time

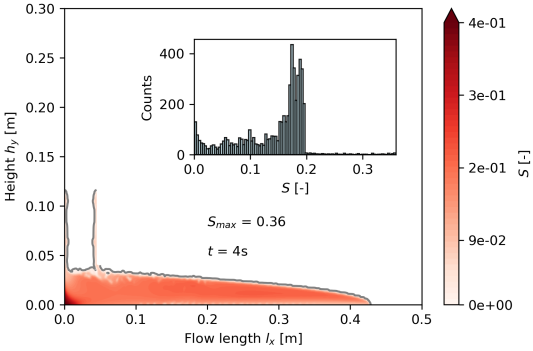

(a) S distribution for T200-a0.1

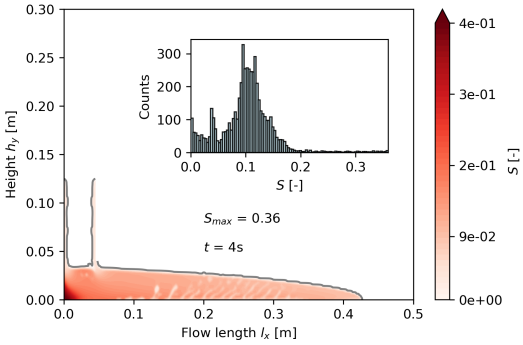

(b) S distribution for T200-a0.2

Figure 9: Effect of deflocculation parameter α on local flow properties

into a CFD simulation to replicate experimental flow tests, and the effect of different thixotropy parameters was tested to assess their impact on simulated flow evolution. Results indicate that both the flocculation time T and defloccation parameter α influence local and transient flow properties especially in time-dependent flow scenarios. While the slump flow test was minimally affected by structural buildup, the L-Box flow decreased with increasing thixotropy values.

It was found that two-dimensional visualization of rheological parameter distributions aids in understanding local and transient flow behavior. Future implementation of thixotropy-dependent rheological models into time-dependent processing simulations will support the understanding and optimization of cement and concrete flow properties.

However, several research questions remain open. Firstly, research must focus on further experimental analysis of structural buildup and breakdown parameters through rheometry and their subsequent integration into numerical frameworks to model thixotropy accurately and close to reality. Secondly, the impact of mathematical regularization techniques for rheological yield stress equations, particularly in the low-flow regime where thixotropy is significant, requires

prospective investigation. Suitable thixotropy-implemented regularization techniques must be explored to address these challenges.

References

[1] S. Amziane, K. Khayat, M. Sonebi, and A. Perrot. Rilem tc 266-mrp: Round-robin rheological tests on high performance mortar and concrete with adapted rheology—evaluating structural build-up at rest of mortar and concrete. *Materials and Structures*, 56(8), 2023.

[2] Ö. Biricik and A. Mardani. Parameters affecting thixotropic behavior of self compacting concrete and 3d printable concrete; a state-of-the-art review. *Construction and Building Materials*, 339:127688, 2022.

[3] J. Brackbill, D. Kothe, and C. Zemach. A continuum method for modeling surface tension. *Journal of Computational Physics*, 100(2):335–354, 1992. PII: 002199919290240Y.

[4] D. C.-H. Cheng and F. Evans. Phenomenological characterization of the rheological behaviour of inelastic reversible thixotropic and antithixotropic fluids. *British Journal of Applied Physics*, 16(11):1599–1617, 1965.

[5] P. Coussot, Q. D. Nguyen, H. T. Huynh, and D. Bonn. Viscosity bifurcation in thixotropic, yielding fluids. *Journal of Rheology*, 46(3):573–589, 2002.

[6] R. de Schryver and G. de Schutter. Insights in thixotropic concrete pumping by a poiseuille flow extension. *Applied Rheology*, 30(1):77–101, 2020.

[7] de Schryver, Robin. *Active rheology control of cementitious materials : numerical and experimental pumping investigation*. Dissertation, Ghent University, 2022.

[8] DIN EN 1015-3:2007-05, Prüfverfahren für Mörtel für Mauerwerk_- Teil_3: Bestimmung der Konsistenz von Frischmörtel (mit Ausbreittisch); EN_1015-3:1999+A1:2004+A2:2006.

[9] DIN EN 12350-10:2010-12, Prüfung von Frischbeton_- Teil_10: Selbstverdichtender Beton_- L-Kasten-Versuch; Deutsche Fassung EN_12350-10:2010.

[10] DIN EN 12350-8:2019-09, Prüfung von Frischbeton_- Teil_8: Selbstverdichtender Beton_- Setzfließversuch, Deutsche Fassung EN_12350-8:2019.

[11] S. Fataei. *Flow-Induced Particle Migration in Concrete under High Shear Rates*. Dissertation, Technische Universität Dresden, 2021.

[12] M. Hosseinpoor, K. H. Khayat, and A. Yahia. Numerical simulation of self-consolidating concrete flow as a heterogeneous material in l-box set-up: coupled effect of reinforcing bars and aggregate content on flow characteristics. *Materials and Structures*, 50(2):346, 2017. PII: 1032.

[13] K. H. Khayat, W. Meng, K. Vallurupalli, and Le Teng. Rheological properties of ultra-high-performance concrete — an overview. *Cement and Concrete Research*, 124:105828, 2019.

[14] S. Ma, Y. Qian, and S. Kawashima. Experimental and modeling study on the non-linear structural build-up of fresh cement pastes incorporating viscosity modifying admixtures. *Cement and Concrete Research*, 108:1–9, 2018.

[15] I. Mehdipour and K. H. Khayat. Understanding the role of particle packing characteristics in rheo-physical properties of cementitious suspensions. *Construction and Building Materials*, 161:340–353, 2018.

[16] T. C. Papanastasiou. Flows of materials with yield. *Journal of Rheology*, 31(5):385–404, 1987.

[17] N. Roussel. A thixotropy model for fresh fluid concretes. *Cement and Concrete Research*, 36(10):1797–1806, 2006.

[18] N. Roussel, H. Bessaies-Bey, S. Kawashima, D. Marchon, K. Vasilic, and R. Wolfs. Recent advances on yield stress and elasticity of fresh cement-based materials. *Cement and Concrete Research*, 124:105798, 2019. PII: S000888461930273X.

[19] N. Roussel, A. Lemaître, R. J. Flatt, and P. Coussot. Steady state flow of cement suspensions. *Cement and Concrete Research*, 40(1):77–84, 2010.

[20] N. Roussel, G. Ovarlez, S. Garrault, and C. Brumaud. The origins of thixotropy of fresh cement pastes. *Cement and Concrete Research*, 42(1):148–157, 2012.

[21] P. Saramito and A. Wachs. Progress in numerical simulation of yield stress fluid flows. *Rheologica Acta*, 56(3):211–230, 2017.

[22] M. Thiedeitz and T. Kränkel. Steady and transient phenomenological thixotropy modeling of non-newtonian cementitious pastes, submitted. *Cement and COncrete Research*, xx(x):xxx–xxx, 2024.

[23] M. Thiedeitz, T. Kränkel, and C. Gehlen. Thixotropy-dependent form filling ability of cement paste. In V. Mechtcherine, K. Khayat, and E. Secrieru, editors, *Rheology and Processing of Construction Materials*, volume 23 of *RILEM Bookseries*, pages 273–280. Springer International Publishing, Cham, 2020.

[24] M. Thiedeitz, T. Kränkel, and C. Gehlen. Viscoelastoplastic classification of cementitious suspensions: transient and non-linear flow analysis in rotational and oscillatory shear flows. *Rheologica Acta*, 61(8-9):549–570, 2022.

[25] M. Thiedeitz, T. Kränkel, D. Kartal, and J. J. Timothy. The slump flow of cementitious pastes: Simulation vs. experiments. *Materials (Basel, Switzerland)*, 17(2), 2024.

[26] L. N. Thrane. *Form Filling with Self-Compacting Concrete*. Dissertation, Technical University of Denmark, Lyngby, 2007.

[27] O. H. Wallevik and J. E. Wallevik. Rheology as a tool in concrete science. *Cement and Concrete Research*, 41(12):1279–1288, 2011.